Proceedings of the ASME 2010 International Manufacturing Science and Engineering Conference
MSEC2010
October 12-15, 2010, Erie, Pennsylvania, USA

MSEC2010-34034

COMBINING PROCESS DYNAMICS AND TOOL WEAR IN THE MILLING SUPER DIAGRAM

Jaydeep Karandikar
University of Florida
Gainesville, FL, USA

Raul Zapata
University of Florida
Gainesville, FL, USA

Tony L. Schmitz
University of Florida
Gainesville, FL, USA

ABSTRACT

This paper describes the milling "super diagram" that incorporates limitations to milling productivity and part quality imposed by stability, surface location error (part errors due to forced vibrations), and tool wear. Combinations of axial depth of cut and spindle speed that offer stable cutting conditions with an acceptable, user-defined surface location error level are identified by a gray-scale color coding scheme. The effect of tool wear is included through the force model coefficients (that relate the cutting force to the chip area) used for process dynamics prediction. Because the force model coefficients vary as a function of the volume of material removed, a unique super diagram is constructed for any user-defined volume of material removed with the selected cutter. For example, preferred operating conditions for a new tool can be compared to those for a worn tool. Additionally, user beliefs about data and model accuracy are applied to identify safety margins relative to the deterministic boundaries in the diagrams.

Experimental results are provided for an inserted (carbide) cutter used to machine 1018 steel. The wear behavior is characterized as changes in the force model coefficients as a function of the volume of material removed. The flank wear is also measured using an on-machine microscope (to avoid tool removal from the spindle) and correlated to the force model coefficients. Stability diagrams are developed that correspond to the new and worn tool performance and experimental results are provided to verify changes in the process stability due to tool wear.

INTRODUCTION

Limitations to milling productivity include tool wear, positioning errors of the tool relative to the part, spindle error motions, fixturing concerns, programming challenges, and the instability introduced by the process dynamics. Many research studies have been completed to address these issues individually. Tobias, Tlusty, and Merrit defined the mechanism for self-excited vibrations (instability) as ''regeneration of waviness'' [1-3]. Other issues related to limitations on milling productivity are detailed in [4-9]. Taylor established an empirical basis for the relationships between cutting parameters and tool wear [10] and subsequent studies have been completed to extend this work. In particular, tool condition monitoring systems have been implemented to estimate tool wear based on various transducer signals [11-12].

In this work, the productivity limits imposed by both the process dynamics and tool wear are considered simultaneously. Information about process dynamics is presented using the milling super diagram [13], which combines stability and surface location error (SLE) information in a graphical format using a gray-scale color coding scheme. The deterministic stability limit [14] and SLE values [15] for a selected spindle speed-axial depth of cut domain are calculated based on the system dynamic response, radial depth of cut, and cutting force model. The effects of tool wear are incorporated here by applying wear-dependent cutting force coefficients [16] to the calculation of the stability limit. By correlating the tool wear status with the change in force coefficient values, the process dynamics can be tailored to the behavior of a new tool or one at or near its end of life. Additionally, model and input data uncertainties are included as a user-specified safety margin. The safety margin captures the user's beliefs regarding how close (in spindle speed and axial depth) he/she is willing to operate relative to the deterministic limits obtained using the frequency-domain models.

SUPER DIAGRAM DESCRIPTION

In previous work, the super diagram combined stability and SLE information without considering the effects of tool

wear. To construct the diagram, the user selected the radial depth of cut, feed per tooth, SLE limit, and spindle speed-axial depth domain. This domain was then discretized into a grid of test points. A penalty was applied to each of the points as follows. Points that were stable and within SLE tolerance levels were not penalized; their value was set to zero. Points that were stable, but outside the SLE tolerance were penalized by one (value = -1). Unstable points were penalized by two (value = -2). The point values for the selected grid were then used to construct a contour plot that served as the super diagram. A gray-scale scheme was used to separate the different zones. The feasible zone (point values = 0) was white, the SLE-limited zones (-1) were gray, and the unstable zone (-2) was black.

In the new super diagram, the cutting force model provided in Eq. 1 is experimentally evaluated as a function of the wear status of the tool. This enables a diagram to be constructed for any level of tool wear depending on the volume of material removed.

$$F_t = K_t bh + K_{te} b$$
$$F_n = K_n bh + K_{ne} b \quad (1)$$

In Eq. 1, F_t is the tangential force component, K_t is the tangential cutting force coefficient, b is the axial depth of cut, h is the instantaneous chip thickness (which depends on the feed per tooth, f_t), K_{te} is the tangential edge (plowing) coefficient, F_n is the normal force component, K_n is the normal cutting force coefficient, and K_{ne} is the normal edge coefficient [8, 9]. It has been previously shown that the force model coefficients tend to increase as wear progresses, e.g., [16]. By correlating the change in these coefficients with wear status, the diagram can be tailored to the behavior of a new tool or one at or near its end of life. The limit between stable/unstable behavior, as well as between acceptable/unacceptable SLE values, was previously indicated using a binary format. To incorporate uncertainty into the super diagram, a user-dependent safety margin is applied to modify the feasible (white) zone. The user selects how close in spindle speed and axial depth he/she is willing to operate relative to the predicted limits. Points within the feasible zone which violate this margin are penalized and a new "safe" feasible zone is identified. A second gray level is now incorporated. Dark gray indicates the stable points where the SLE limit is exceeded, while light gray represents the previously feasible points which violate the safety margin.

NUMERICAL CASE STUDY

To demonstrate the super diagram including tool wear and uncertainty, a numerical case study was completed. The parameters are provided in Table 1. The original diagram for the selected system is shown in Fig. 1, where the surface location error limit is 50 μm.

Tool life is traditionally specified by the time required to reach a pre-selected wear level, often quantified using flank wear width (FWW). The FWW tends to increase with volume removed and is cutting speed (spindle speed) dependent. The assumed relationship between FWW and volume removed for the numerical example is shown in Fig. 2, where the tool life is defined as the time to reach a FWW of 0.3 mm.

Table 1: Numerical case study parameters.

Parameter	Value	Units
Stiffness	5×10^6	N/m
Damping ratio	0.05	
Natural frequency	300	Hz
Tool diameter	19.05	mm
Helix angle	0	degrees
Number of teeth	1	
Tangential cutting coefficient	2×10^9	N/m^2
Normal cutting coefficient	0.667×10^9	N/m^2
Feed per tooth	0.06	mm/tooth
Radial depth of cut	4.725	mm

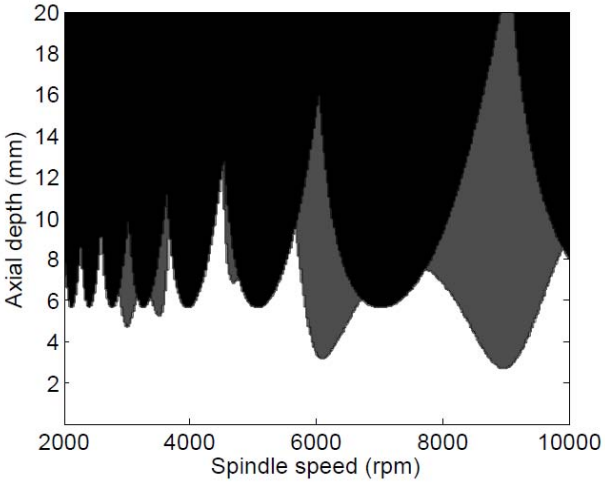

FIGURE 1: SUPER DIAGRAM WITH 50 μm SLE LIMIT.

As noted, the cutting forces tend to grow with FWW. The assumed relationships between the cutting coefficients, K_t and K_n, identified in Eq. 1 and the volume removed are provided in Figs. 3 and 4. The assumed linear relationship between these coefficients, spindle speed, Ω, and volume removed, V, is provided in Eq. 2, where the intercepts, $c_{0,t}$ and $c_{0,n}$, are the new tool coefficients (Table 1), and $c_{1,t}$ and $c_{1,n}$ are the speed-dependent rates of increase with V.

$$K_t(\Omega, V) = c_{0,t} + c_{1,t} V$$
$$K_n(\Omega, V) = c_{0,n} + c_{1,n} V \quad (2)$$

These slopes were assumed to increase linearly with Ω between 2000 rpm and 10000 rpm such that the coefficients doubled at 10000 rpm for $V = 20$ cm^3 (where FWW = 0.3 mm; see Fig. 2) with no change at 2000 rpm for the same V. As an example, for Ω = 3000 rpm with $V = 20$ cm^3,

$c_{1,t} = \frac{c_{0,t}}{V}\frac{3000-2000}{10000-2000} =$ 1.25x10^7 N/m^2/cm^3, by linear interpolation and $K_t = 2.0\times10^9 + 1.25\times10^7 V = 2.25\times10^9$ N/m^2. Given this relationship between cutting coefficients, V, and Ω, the super diagram can then be modified to incorporate tool wear (the edge coefficients are not included in this example without loss of generality). As before, the {Ω, b} domain is represented by a grid of points and the stability and SLE is determined for each point. However, in this case, the volume to be removed must first be selected by the user. Then, the coefficients can be calculated for each spindle speed and, subsequently, the stability limit can be determined. Also, SLE is calculated at each axial depth grid point for the given spindle speed. The new diagram for V = 20 cm^3 is provided in Fig. 5. Because the cutting coefficients grow with Ω, the stability limit decreases and the SLE infeasible zone grows while moving from left to right in the diagram.

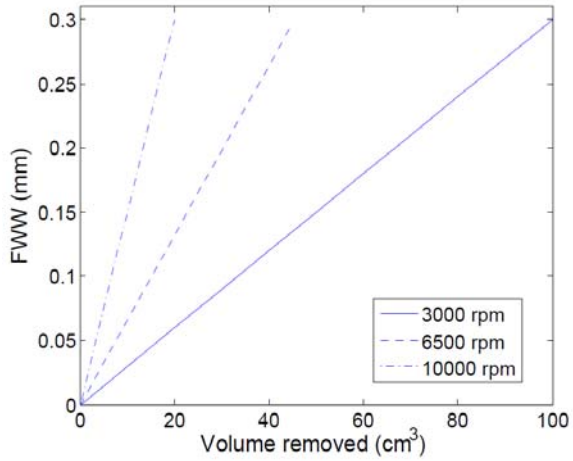

FIGURE 2: VARIATION IN FWW WITH *V* AT DIFFERENT SPEEDS.

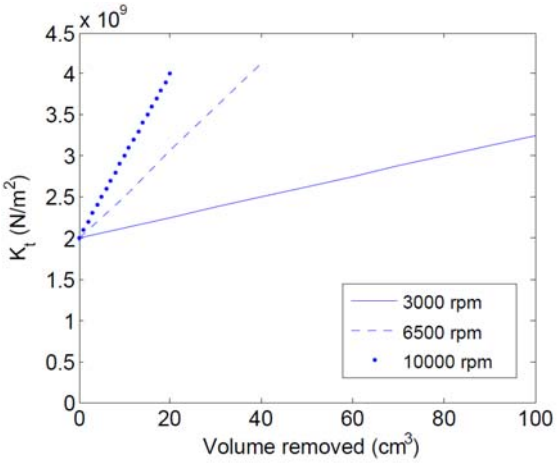

FIGURE 3: VARIATION IN K_t WITH *V* AT DIFFERENT SPEEDS.

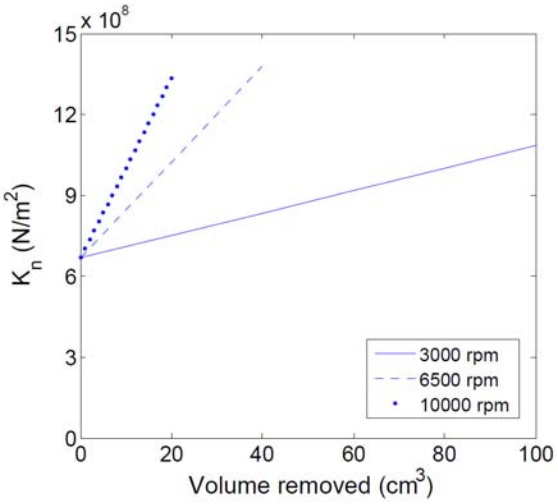

FIGURE 4: VARIATION IN K_n WITH *V* AT DIFFERENT SPEEDS.

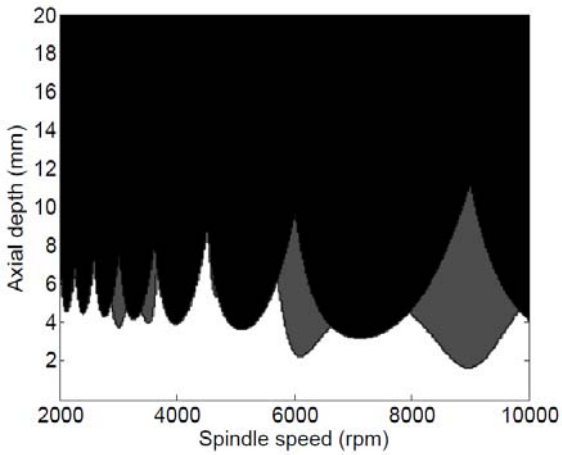

FIGURE 5: SUPER DIAGRAM INCLUDING TOOL WEAR EFFECTS (V = 20 cm^3).

Next, the super diagram was modified to incorporate the user's beliefs regarding uncertainty in the actual location of the deterministic boundaries. To carry out this task, the user defines safety limits for spindle speed, ΔΩ, and axial depth of cut, Δb. These values give the distances from the boundaries that represent his/her 95% confidence level for actual feasible performance. For each feasible point in the {Ω, b} domain defined by the white zone, the penalty value of the surrounding eight points at distances ΔΩ and Δb from the test point are queried (see Fig. 6). If any of these points are infeasible (with a penalty of -1 or -2), then the test point is penalized and also identified as infeasible as shown in Fig. 6.

A new gray-scale is then implemented where the point values are: feasible (0, white), safety margin (-1, light gray), SLE limit (-2, dark gray), and unstable (-3, black). Therefore, the (white) feasible zone is reduced after the application of the

user-specified safety margins. Figure 7 shows a super diagram with safety margins of $\Delta\Omega = 100$ rpm and $\Delta b = 0.5$ mm.

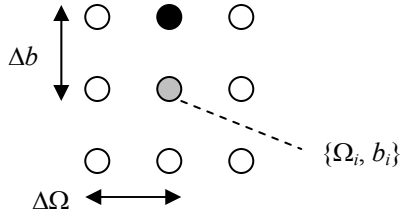

FIGURE 6: THE SAFETY LIMIT IS IDENTIFIED BY TESTING THE FEASIBILITY OF THE EIGHT GRID POINTS SURROUNDING {Ù$_i$, b_i}. IN THIS CASE, THE TEST POINT IS PENALIZED (-1) BECAUSE THE (BLACK) POINT ABOVE IT IS UNSTABLE.

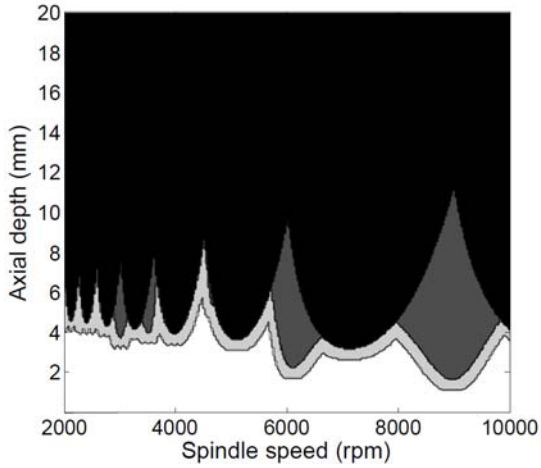

FIGURE 7: SUPER DIAGRAM INCLUDING TOOL WEAR EFFECTS AND THE USER-DEFINED SAFETY MARGIN (V = 20 cm^3, $\Delta\Omega$ = 100 rpm, and Δb = 0.5 mm).

TOOL WEAR EXPERIMENTS

The experimental steps followed to collect the tool wear data for a 19 mm diameter inserted endmill (one square uncoated Kennametal 107888126 C9 JC carbide insert; zero rake and helix angles, 15 deg relief angle, 9.53 mm square x 3.18 mm) are described here. The workpiece material was 1018 steel. An atomic force microscope (AFM) was used to measure the topography of the carbide inserts. Figure 8 shows an example 50 μm x 50 μm measurement (256 line scans, no digital filtering) of the rake face. It is seen that there is a small chamfer with a 167 deg angle at the cutting edge. The roughness average for the rake face is 310 nm.

The first test was completed at a spindle speed, Ω, of 2500 rpm with a 3 mm axial depth of cut and 4.7 mm radial depth of cut (25% radial immersion). The feed per tooth value was 0.06 mm/tooth. The four coefficients in Eq. 1 were evaluated by performing a linear regression to the mean x (feed) and y direction forces obtained over a range of feed per tooth values: f_t = {0.03, 0.04, 0.05, 0.06, and 0.07} mm/tooth [9]. The cutting forces were monitored using a table-mounted force dynamometer (Kistler 9257B). In addition to calculating the cutting force coefficients intermittently while wearing the tool, the insert wear profile was also recorded at these intervals. To avoid removing the insert/tool from the spindle, a handheld microscope (60x magnification) was fixtured inside the machine enclosure and was used to measure the rake and flank surfaces. The calibrated digital images were used to identify the flank wear width (FWW). No crater wear was observed.

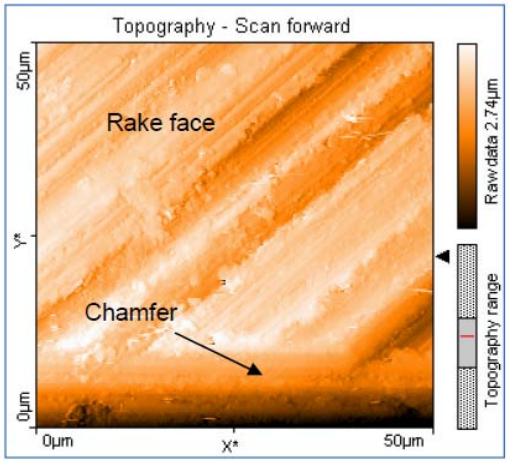

FIGURE 8: TYPICAL AFM MEASUREMENT OF CARBIDE INSERT RAKE FACE.

Microscope images of the relief face for selected volumes of material removed, V, are shown in Fig. 9. The sequence of tests was repeated three times to evaluate the repeatability from one insert to the next. Figure 10 shows the increase in maximum FWW with volume removed; one standard deviation (1σ) error bars are also included. The measurements were completed at increments of 12 cm^3. The force coefficients were also calculated using the linear regression approach at each interval. These results are shown in Figs. 11 and 12.

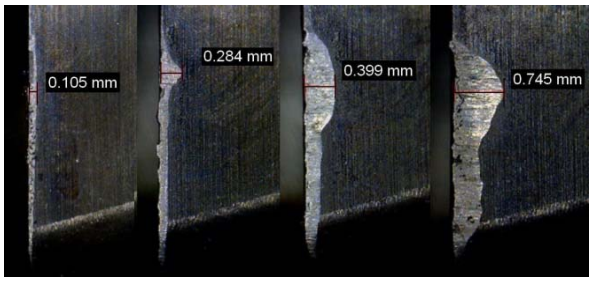

FIGURE 9: IMAGES OF INSERT RELIEF FACE AT 60X MAG NIFICATION (FROM LEFT TO RIGHT, V = {50, 125, 200, and 275} cm^3).

It can be seen from Fig. 11 that K_t and K_n increased with tool wear, while Fig. 12 shows that the K_{te} and K_{ne} values

exhibited no clear trend. Additionally, the distributions in K_t and K_n values increased with tool wear. For the selected tool/material pair, there was an approximately linear growth in K_t and K_n (R^2 values of 0.877 and 0.853 for K_t and K_n, respectively).

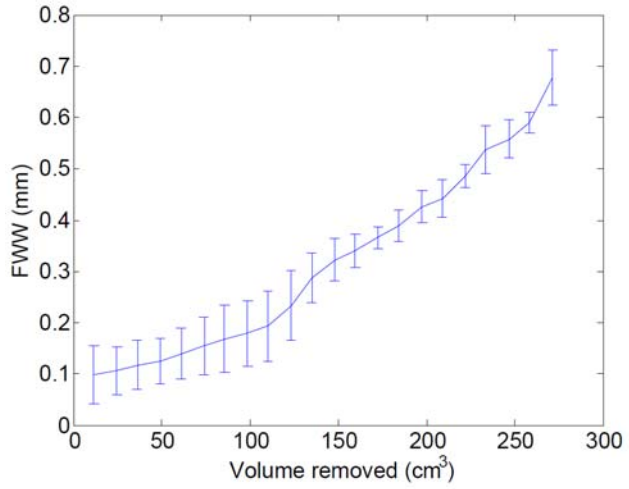

FIGURE 10: VARIATION IN FWW WITH V (Ω = 2500 rpm).

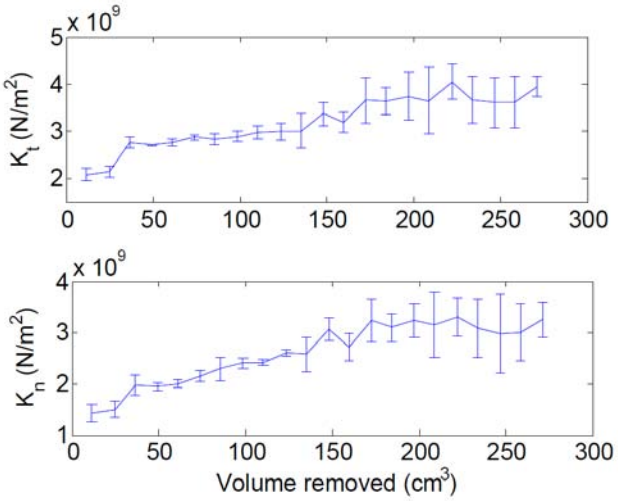

FIGURE 11: VARIATION IN K_t AND K_n WITH V (Ω = 2500 rpm).

Next, additional tests were carried out at spindle speeds of {3750, 5000, 6250, and 7500} rpm. The procedure and parameters (other than spindle speed) were the same as described for the 2500 rpm testing. The results are displayed in Fig. 13; the linear least squares fits to the data are also shown. It is seen that the growth rates of K_t and K_n with volume removed (i.e., the slopes of the lines) increase with spindle speed. Interestingly, when plotted versus the corresponding FWW (measured with the microscope), the five different spindle speed results collapse onto a single line; see Fig. 14. This suggests that if the FWW were monitored, it could provide an in-process approach to updating the force model coefficients based on the tool wear status. The K_{te} and K_{ne} values again did not exhibit any significant trend.

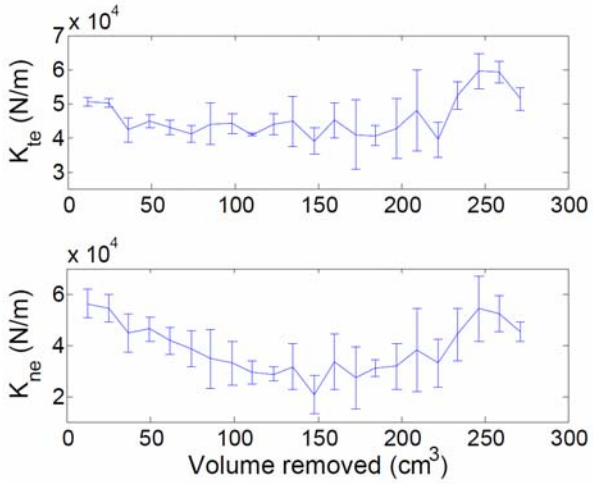

FIGURE 12: VARIATION IN K_{te} AND K_{ne} WITH V (Ω = 2500 rpm).

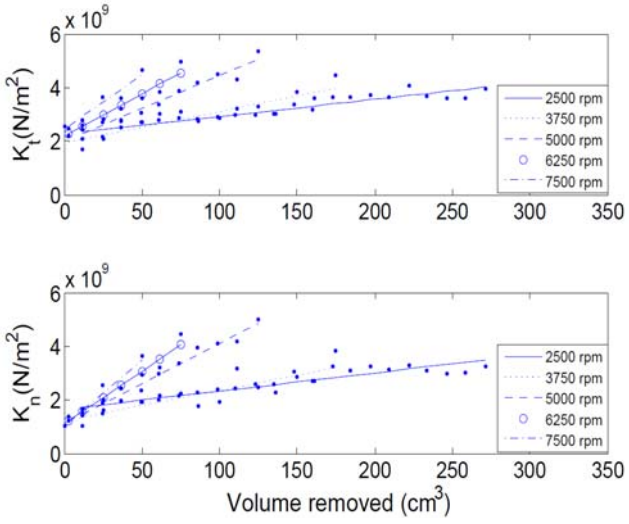

FIGURE 13: VARIATION IN K_T AND K_N WITH V FOR Ω = {2500, 3750, 5000, 6250, and 7500} rpm.

To describe the variation in K_t and K_n with volume removed as a function of spindle speed, the slopes of the individual lines in Fig. 13 are plotted against spindle speed in Fig. 15. As seen from the figure, the slopes increase linearly with spindle speed. The error bars in the figure were obtained from Monte Carlo simulation, where random values of K_t and K_n (within the 1σ range) were selected for each volume and a line was fit to this combination. The slope was calculated for each line and the mean and standard deviation for each spindle speed was used to construct Fig. 15.

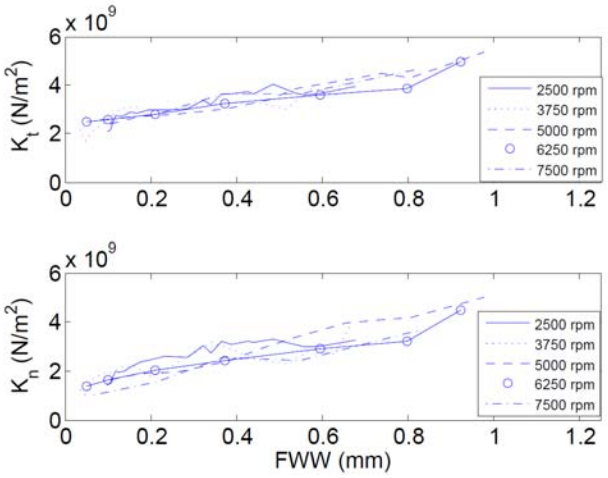

FIGURE 14: VARIATION IN K_t AND K_n WITH FWW FOR Ω = {2500, 3750, 5000, 6250, and 7500} rpm.

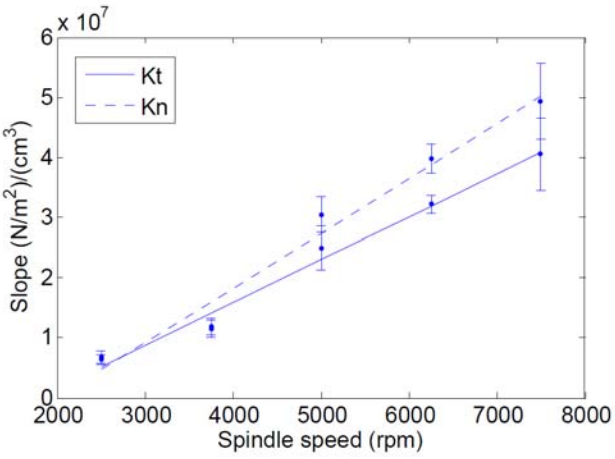

FIGURE 15: VARIATION IN SLOPE WITH SPINDLE SPEED FOR THE K_t AND K_n VERSUS V LINES FROM FIG. 13.

Using Figs. 13 and 15, the increase in force coefficients K_t and K_n with spindle speed and volume removed can be expressed using the linear relationships given by Eq. 2. In this equation, $c_{0,t}$ and $c_{0,n}$, are the coefficient values for a new tool (V = 0 in Fig. 11). The speed-dependent rates of increase, $c_{1,t}$ and $c_{1,n}$,are calculated using the slopes and intercepts of the lines in Fig. 15. The slopes are 7.1×10^3 (N/m^2/cm^3)/rpm and 9.1×10^3 (N/m^2/cm^3)/rpm and the intercepts are -1.3×10^7 N/m^2/cm^3 and -1.8×10^7 N/m^2/cm^3 for the K_t and K_n data, respectively. The negative intercept values are attributed to the linear fit with inherent experimental uncertainty. The terms $c_{1,t}$ and $c_{1,n}$ are defined at different speeds by multiplying the slope by the corresponding spindle speed and adding the intercept as shown in Eq. 3. For the given tool-material combination, the increase in force coefficients at any spindle speed-volume removed combination within the testing range can be calculated using this equation. The coefficients can then be used to develop a super diagram that accounts for tool wear effects.

$$K_t(\Omega,V) = c_{0,t} + \left(7.1\times10^3 - 1.3\times10^7\right)V$$
$$K_n(\Omega,V) = c_{0,n} + \left(9.1\times10^3 - 1.8\times10^7\right)V \quad (3)$$

The previous tests were performed at f_t = 0.06 mm/tooth. This enables the coefficients to be evaluated at that value. However, changing the feed per tooth can affect the wear rate and SLE values. Therefore, a similar set of experiments was completed at f_t = {0.03, 0.045, 0.075, and 0.09} mm/tooth. The tests were completed at 5000 rpm with all other parameters held constant. Figure 16 shows the variation in cutting force coefficients with volume removed for these feed per tooth values.

The wear rate is higher and the volume of material that can be removed is lower for the smaller feed per tooth values. This wear rate trend suggests that strain hardening may be in effect. The thinner chips with increased hardness can cause accelerated wear. The reduced amount of material that can be removed could also be attributed to the increase in cutting time and the number of passes through the material required to remove the same volume for smaller feed per tooth values.

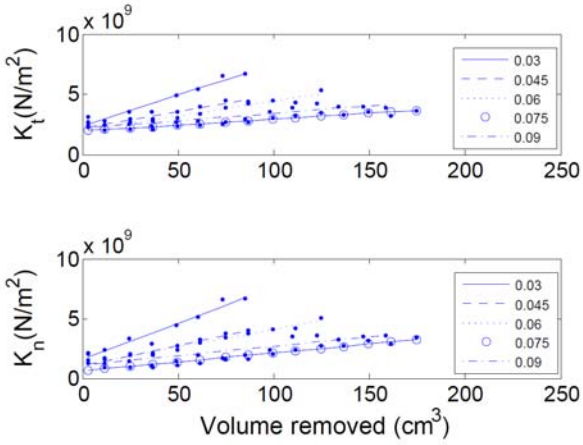

FIGURE 16: VARIATION IN K_t AND K_n WITH V FOR f_t = {0.03, 0.045, 0.06, 0.075 and 0.09} mm/TOOTH.

Finally, the variation in wear rate behavior with axial depth of cut was evaluated. The axial depths were {3, 4.5, and 6} mm, the spindle speed was 5000 rpm, the feed per tooth was 0.06 mm/tooth and the radial depth remained at 4.7 mm. Figure 17 shows the results. Note that the K_t and K_n values are plotted against volume normalized by the axial depth of cut, $V_n = V/b$. This normalization was necessary because the independent variable, V, is a function of the dependent variable, b. As seen in the figure, the three test sets collapse onto a single line for the usable tool life when plotted versus the normalized volume. It has also been suggested that variation in FWW is not

observed at different radial depths of cut and differing number of teeth (assuming no runout) [5].

By normalizing the volume removed by the axial and radial depths of cut and number of teeth, the required number of tests can be dramatically reduced. For a given tool-workpiece combination, testing can therefore be completed only at a selected axial depth of cut, radial depth of cut, and number of teeth. The results can then be extended to other combinations by plotting the values of force coefficients against the normalized volume removed.

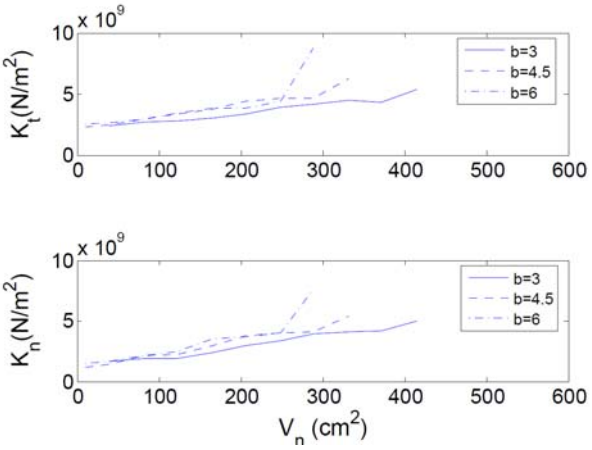

FIGURE 17: VARIATION IN K_t AND K_n WITH NORMALIZED VOLUME REMOVED FOR b = {3, 4.5, and 6} mm.

EXPERIMENTAL VALIDATION

The tool wear experimental results showed a linear increase in cutting force coefficients K_t and K_n with volume removed due to progressive flank wear. The rate of increase of force coefficients increased linearly with speed. This increase in force coefficients causes the limiting axial depth of cut to decrease. To explore this wear effect, the tool point frequency response function was measured by impact testing and the stability limit was calculated using force coefficients based on a new and worn insert. An insert was worn by removing 275 cm^3 at Ω = 2500 rpm. The force coefficients were determined for both a new insert and the worn insert using a linear regression of the average x and y direction forces at varying feed per tooth values as described previously. These force coefficients are provided in Table 2. For stability testing at 5100 rpm, the equivalent volume removed which would yield the K_t and K_n values for the worn insert was calculated to be 121 cm^3 using Eq. 3. The stability limit for the new insert was calculated using the new insert values (V = 0). For the worn insert, the K_t and K_n values at each spindle speed were calculated using Eq. 3 and the stability limit was generated as described in the numerical study. However, as shown by the error bars in Fig. 15, there is uncertainty in the K_t and K_n values for both the new and worn inserts. A Monte Carlo simulation was completed where random K_t and K_n values were selected from the experimental distributions and a new stability limit was calculated for each set. See Fig. 18, where the radial depth of cut is equal to the tool diameter (slotting). The band of stability limits indicates the uncertainty. This information could be used, for example, to aid a user in selecting his/her safety limits for the super diagram. The mean limiting depth of cut at 5100 rpm is 2.15 mm for the new insert and 0.85 mm for the worn insert.

Table 2: Force coefficient values for new and worn inserts.

	K_t (N/m^2)	K_n (N/m^2)	K_{te} (N/m)	K_{ne} (N/m)
New	1.90 x 10^9	0.78 x 10^9	45500	46650
Worn	4.98 x 10^9	4.51 x 10^9	45500	25500

Cutting tests were completed at b = {0.8, 1.6, 2.2, and 3} mm with the new and worn inserts. A once-per-revolution force sampling strategy for the x (F_x) and y (F_y) directions was used to identify chatter. The once-per-revolution samples were obtained by sampling the force data at the commanded spindle rotating frequency. For stable cutting conditions, the once-per-revolution samples (due to forced vibration only) are synchronous with spindle rotation and produce a small cluster of points [17] in the F_x vs. F_y plot. Unstable behavior, on the other hand, produces a more distributed set of points due to its asynchronous nature. A statistical variance ratio, R, is used as an indicator of chatter [18]; see Eq. 4, where $\sigma^2_{opr,x}$ and $\sigma^2_{opr,y}$ are the variances in the once-per-revolution sampled forces in the x and y directions and σ^2_x and σ^2_y are the variances in the x and y direction forces. Figure 19 shows once-per-revolution samples for tests at b = 1.6 mm and Ω = 5100 rpm for the new and worn inserts.

$$R = \frac{\sigma^2_{opr,x} + \sigma^2_{opr,y}}{\sigma^2_x + \sigma^2_y} \tag{4}$$

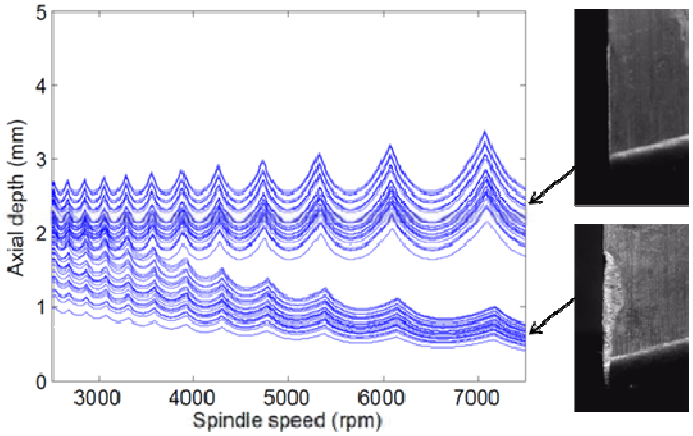

FIGURE 18: STABILITY LOBE DIAGRAM FOR NEW (V = 0) AND WORN INSERTS (V = 121 cm^3).

As seen in Fig. 19, the distribution of once-per-revolution samples increases for the unstable cut using the worn insert. Similar results were obtained b = 0.8 mm (which is within the

stability limit distribution for the worn tool in Fig. 18), 2.2 mm, and 3 mm. Figure 20 shows the R values for different axial depths of cut, where the R value is larger for all cuts with the worn insert and increases substantially for both the new and worn insert at b = 3 mm (violent chatter occurred in both cases for this depth). Sample surface profiles for Ω = 5100 rpm with b = 1.6 mm for the new and worn inserts corroborate the R results. Figures 21 and 22 display the topography of the machined surface obtained using a scanning white light interferometer with a 10x magnification and 2.5 mm by 1 mm field of view. The unstable condition for the worn insert produces the expected rough surface finish. The average surface roughness for Fig. 21 is 781.8 nm; this surface does not show any distinct chatter marks. The average surface roughness for the unstable result (worn tool) in Fig. 22 is 4018.5 nm (5.1 times increase) and the surface exhibits chatter marks. These results indicate that the stability limit did decrease with increased tool wear.

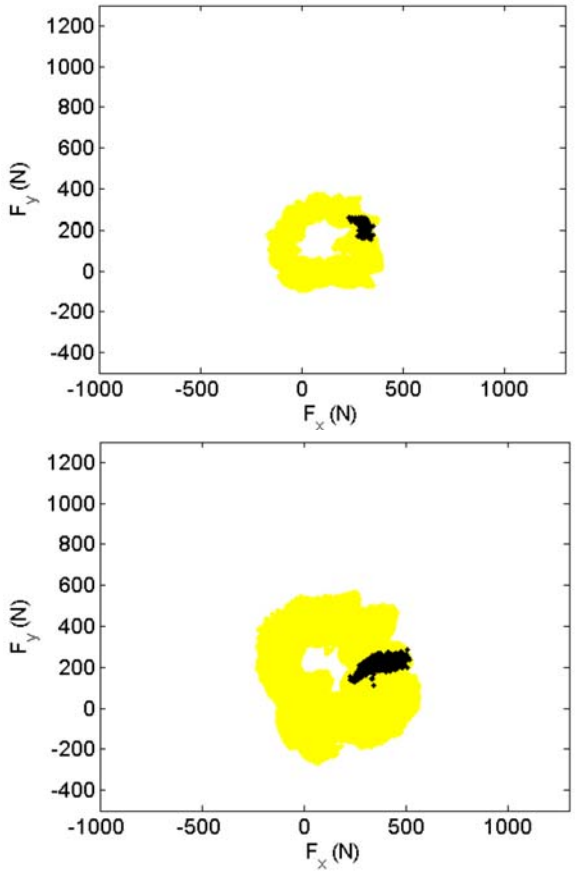

FIGURE 19: ONCE-PER-REVOLUTION SAMPLES FOR 1.6 mm AXIAL DEPTH OF CUT AND 5100 rpm SPINDLE SPEED (TOP: NEW INSERT, BOTTOM: WORN INSERT).

CONCLUSIONS

In this work, the effect of tool wear on milling stability was evaluated experimentally. By modifying the force model coefficients according to the wear status (as a function of volume removed), tool wear effects were incorporated into the milling super diagram. Tests were completed to establish the variation in cutting force coefficients with tool wear as a function of spindle speed and volume removed for a zero rake/zero helix/15 deg relief angle, square, uncoated carbide insert used to machine 1018 steel. The single insert was mounted in a 19 mm diameter steel tool body. For this tool-material pair, it was observed that the cutting coefficients, which relate the tangential and normal force components to chip area, increased linearly with volume removed and the corresponding slope increased linearly with spindle speed. However, the edge (plowing) coefficients, that relate the forces to chip width only, showed no appreciable trend with tool wear. Cutting tests were completed to verify the change in process stability with tool wear status.

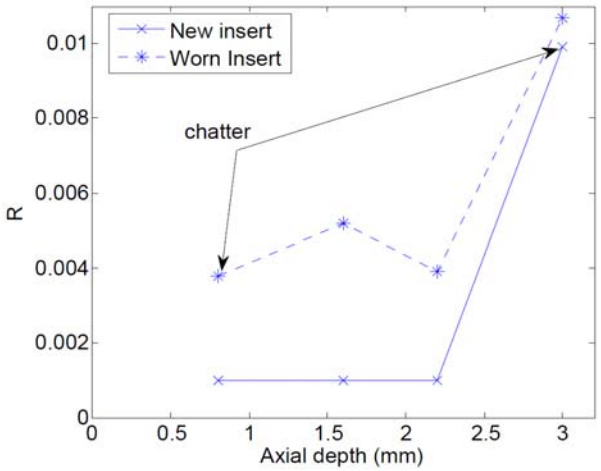

FIGURE 20: VARIANCE RATIO, *R*, FOR NEW AND WORN INSERTS AT DIFFERENT AXIAL DEPTHS OF CUT.

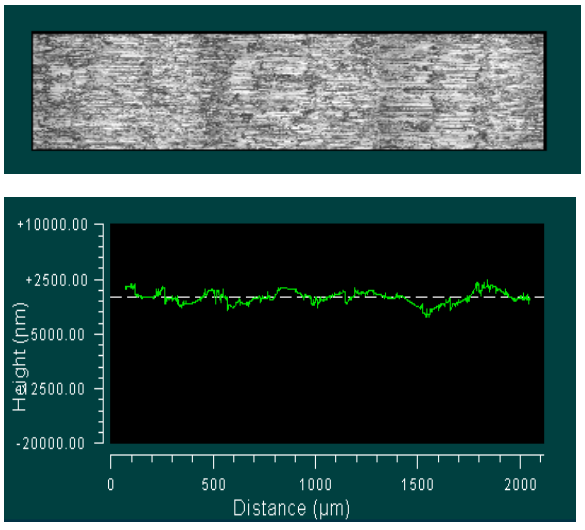

FIGURE 21: SURFACE PROFILE FOR NEW INSERT (STABLE CUTTING) FOR 5100 rpm WITH *b* = 1.6 mm.

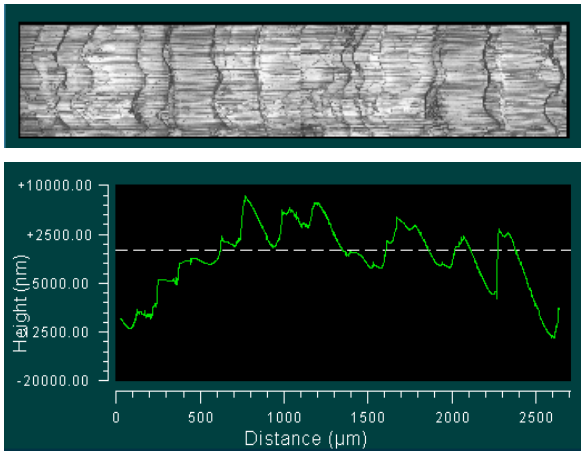

FIGURE 22: SURFACE PROFILE FOR WORN INSERT (UNSTABLE) FOR 5100 rpm with *b* = 1.6 mm.

ACKNOWLEDGEMENTS

The authors gratefully acknowledge partial financial support from the National Science Foundation (CMMI-0926667) and Kennametal (donation of carbide inserts).

REFERENCES

1. Tobias, S.A. and Fishwick, W., 1958, "The Chatter of Lathe Tools under Orthogonal Cutting Conditions," Transactions of the ASME, 80, pp. 1079.
2. Tlusty, J. and Polocek, M., 1963, "The Stability of the Machine-Tool against Self-Excited Vibration in Machining," In: Proceedings of the International Research in Production Engineering Conference, Pittsburgh, PA, ASME, New York, NY, pp. 465.
3. Merrit, H., 1965, "Theory of Self-Excited Machine Tool Chatter," Journal of Engineering for Industry, Transactions of the ASME, 87(4), pp. 447-454.
4. Tlusty, J., 2000, Manufacturing Processes and Equipment. Prentice Hall, Upper Saddle River, NJ.
5. Trent, E. and Wright, P., 2000, Metal Cutting 4th Ed., Butterworth Heinemann, Boston, MA.
6. Dornfeld, D. and Lee, D.E., 2008, Precision Manufacturing, Springer, New York, NY.
7. Slocum, A., 1992, Precision Machine Design, Prentice-Hall, Inc., Englewood Cliffs, NJ.
8. Altintas, Y., 2000, Manufacturing Automation, Cambridge University Press, Cambridge, UK.
9. Schmitz, T. and Smith, K.S., 2009, Machining Dynamics: Frequency Response to Improved Productivity, Springer, New York, NY.
10. Taylor, F.W., 1906, "On the Art of Cutting Metals." Transactions of the ASME, 28, pp. 31-248.
11. Prickett, P. and Johns, C., 1999, "An Overview of Approaches to End Milling Tool Monitoring," International Journal of Machine Tools and Manufacture, 39, pp. 105–122.
12. Rehorn, A., Jiang, J. and Orban, P., 2005, "State-of-the-art Methods and Results in Tool Condition Monitoring: A Review," International Journal of Advanced Manufacturing Technology, 26, pp. 693–710.
13. Zapata, R., Karandikar J. and Schmitz T., 2009, "A New 'Super Diagram' for Describing Milling Dynamics." Transactions of NAMRI/SME, 36, pp. 245-252.
14. Altintas, Y. and Budak, E., 1995, "Analytical Prediction of Stability Lobes in Milling." Annals of the CIRP, 44(1), pp. 357-362.
15. Schmitz, T. and Mann B., 2006, "Closed Form Solutions for Surface Location Error in Milling." International Journal of Machine Tools and Manufacture, 46, pp. 1369-1377.
16. Cui, Y., Fussell, B., Jerard, R., and Esterling, D., 2009, "Tool Wear Monitoring for Milling by Tracking Cutting Force Model Coefficients," Transactions of the NAMRI/SME, 37, pp. 613-620.
17. Davies M., Dutterer B., Pratt J., Schaut A., and Bryan J., 1998, "On the Dynamics of High-Speed Milling with Long, Slender Endmills," Annals of the CIRP, 47(1), pp. 55-60.
18. Cheng C., Schmitz T. L. and Duncan G. S, 2007, "Rotating tool point frequency response prediction using RCSA," Machining Science and Technology, 11, pp. 433-446.